Nanoscale

ROYAL SOCIETY OF CHEMISTRY

PAPER

View Article Online
View Journal | View Issue

Check for updates

Cite this: *Nanoscale*, 2024, **16**, 887

Turning cationic antimicrobial peptide KR-12 into self-assembled nanobiotics with potent bacterial killing and LPS neutralizing activities†

Ruyi Lei,*‡[a] Chujun Yang, ‡[a,b] Yaqi Sun,‡[c] Dejian Li,[a] Liman Hao,[d] Yang Li,[d] Shuijing Wu,[d] Hui Li,[d] Chao Lan*[a] and Xiangming Fang*[d]

Gram-negative sepsis has become a substantial and escalating global healthcare challenge due to the growing antibiotic resistance crisis and the sluggish development of new antibiotics. LL-37, a unique Cathelicidin species found in humans, exhibits a wide range of bioactive properties, including direct bactericidal effects, inflammation regulation, and LPS neutralization. KR-12, the smallest yet potent peptide fragment of LL-37, has been modified to create more effective antimicrobials. In this study, we designed two myristoylated derivatives of KR-12, referred to as Myr-KR-12N and Myr-KR-12C. These derivatives displayed remarkable ability to spontaneously assemble into nanoparticles when mixed with deionized water. Myristoylated KR-12 derivatives exhibited broad-spectrum and intensified bactericidal activity by disrupting bacterial cell membranes. In particular, Myr-KR-12N showed superior capability to rescue mice from lethal *E. coli*-induced sepsis in comparison with the conventional antibiotic meropenem. We also confirmed that the myristoylated KR-12 nanobiotic possesses significant LPS binding capacity and effectively reduces inflammation *in vitro*. In an *in vivo* context, Myr-KR-12N outperformed polymyxin B in rescuing mice from LPS-induced sepsis. Crucially, toxicological assessments revealed that neither Myr-KR-12N nor Myr-KR-12C nanobiotics induced meaningful hemolysis or caused damage to the liver and kidneys. Collectively, our study has yielded an innovative nanobiotic with dual capabilities of bactericidal action and LPS-neutralization, offering substantial promise for advancing the clinical translation of antimicrobial peptides and the development of novel antibiotics. This addresses the critical need for effective solutions to combat Gram-negative sepsis, a pressing global medical challenge.

Received 13th October 2023,
Accepted 3rd December 2023

DOI: 10.1039/d3nr05174a

rsc.li/nanoscale

1. Introduction

Gram-negative sepsis unfolds as a consequence of an unbridled immune response triggered by infection. In this intricate cascade, immune cells become activated by lipopolysaccharides (LPS) emanating from the bacterial outer membrane, inciting a vigorous inflammatory reaction culminating in organ failure, pronounced inflammation, and potential lethality.[1] This ailment has burgeoned into a substantial and escalating global healthcare burden, presenting a formidable challenge to researchers and intensive care clinicians, owing to its high and burgeoning prevalence, intricate genetic, pathophysiological, and clinical nuances.[2] The escalating issue of antibiotic resistance, coupled with the sluggish pace of novel antibiotic development, necessitates an expeditious quest for innovative antimicrobial agents.[3,4]

In this context, antimicrobial peptides (AMPs), which are naturally occurring peptides endowed with therapeutic attributes within the innate immune system, warrant profound consideration. Characterized by their amphiphilic nature and ranging in length from 10 to 50 amino acids, these peptides bear a net positive charge (2–9 in terms of net charge).[5] Derived from a myriad of sources including unicellular bacteria, plants, amphibious animals, and even mammals, including humans, AMPs occupy a pivotal role as the vanguard of host defense against invading microorganisms.[6] A wealth of such peptides have been identified and cataloged within the antimicrobial peptide database.[7] Diverging from conventional antibiotics, which typically exhibit bactericidal effects and target specific cellular components, AMPs exert their bactericidal impact through membrane disruption while simul-

[a]*Department of Emergency Medicine, The First Affiliated Hospital of Zhengzhou University, Zhengzhou 450052, China. E-mail: ruyilei@zzu.edu.cn, lanchao29@163.com*
[b]*Academy of Medical Sciences, Zhengzhou University, Zhengzhou 450052, China*
[c]*China National Clinical Research Center for Child Health, Children's Hospital, Zhejiang University School of Medicine, Hangzhou 310052, China*
[d]*Department of Anesthesiology, The First Affiliated Hospital, School of Medicine, Zhejiang University, Hangzhou 310003, China. E-mail: xmfang@zju.edu.cn*
†Electronic supplementary information (ESI) available. See DOI: **https://doi.org/10.1039/d3nr05174a**
‡These authors contributed equally to this work.

taneously engaging multiple cellular targets.[8] Consequently, they are less prone to inducing bacterial resistance.[9–11] Furthermore, their immune-modulatory properties and regulation of microbial ecosystems have been documented.[8] However, the clinical application of AMPs is impeded by several key factors, such as susceptibility to the bactericidal activity of salt solutions, vulnerability to hydrolysis by proteases, as well as concerns regarding *in vivo* toxicity, along with high production costs.[12] Consequently, an increasing number of studies have been undertaken to optimize the modification of natural AMPs. This optimization involves the introduction of non-natural amino acids, lipidation modification, cyclization, and nanomodification.[10–12] These endeavors aim to overcome the limitations associated with natural AMPs and design novel antimicrobial drugs characterized by robust bactericidal efficacy, stability, and low toxicity. Such innovations are poised to offer new antimicrobial strategies for clinical applications.

The family of AMPs known as Cathelicidins has been unearthed across various mammalian species. In humans, the sole representative is LL-37, primarily expressed within epithelial and immune cells. Beyond its direct pathogen-killing attributes, LL-37 boasts a repertoire of additional biological activities encompassing the regulation of inflammation and neutralization of LPSs.[13,14] LL-37 exerts a moderate antibacterial efficacy against a wide spectrum of both Gram-negative and Gram-positive bacteria. Its antibacterial action manifests through both direct bactericidal effects and immunomodulatory mechanisms, with membrane disruption being the primary mode of action. KR-12, comprising residues 18 to 29 of LL-37, stands as the smallest yet potent peptide fragment of LL-37, renowned for its pivotal role in conferring the antimicrobial and anti-inflammatory attributes to the LL-37 peptide.[15,16] Notably, when juxtaposed with the full-length LL-37, KR-12 presents superior cell selectivity while also offering the advantage of reduced manufacturing costs. This juxtaposition underscores the potential for optimizing therapeutic interventions based on this truncated LL-37 derivative.[17,18]

Recent years have witnessed a burgeoning interest in modifying members of the Cathelicidin family to yield antibacterial therapeutics with diverse functions. Demonstrations of therapeutic efficacy have been witnessed in rat septic shock models employing a sheep myeloid antimicrobial peptide (SMAP)-29, derived from Cathelicidin, equating its anti-endotoxic potency to polymyxin B.[19] Lipopeptides originating from KR-12 have demonstrated superior bactericidal efficacy in both *in vitro* settings and in treating MRSA infections *in vivo*.[20] Moreover, enhancements in the hydrophobicity of a KR-12 analog have yielded more efficacious bactericidal agents *in vivo*.[21] A previous study, focused on amino acid substitutions, has underscored their differential effects against various organisms.[22,23]

In the realm of nanotechnology, nanoscale structures have been meticulously crafted through the noncovalent self-assembly of individual molecules, offering a gamut of applications in biomedicine.[24] For instance, nanotechnology has been harnessed to convert a human alpha defensin-5 peptide into a potent antibacterial agent.[25] Another study employed nanotechnology to modify a mutant fragment of LL-37, resulting in micelles possessing robust antifungal activity. Additionally, through the utilization of peptide-linked PLGA conjugate micelles, the antitumor efficacy of an analog of the LL-37 peptide fragment was significantly augmented.[26] The present study involves the design and synthesis of a suite of peptides derived from KR-12, with the aim of assessing their therapeutic efficacy and *in vitro* and *in vivo* toxicological profiles. The outcome of this endeavor is a novel nanobiotic surpassing meropenem in an *in vivo* mouse sepsis model and outperforming polymyxin in LPS neutralization. Our findings hold the potential to inform the development of groundbreaking antibiotics.

2 Methods

2.1 Synthesis of peptides

Peptides were synthesized *via* solid-phase peptide synthesis (SPPS) by Shanghai Top Bio Co., Ltd, employing Fmoc chemistry on an automated peptide synthesizer. Rink Amide MBHA resin acted as the solid support, and Fmoc-protected amino acids, HBTU, HOBt, and DIPEA, were utilized for coupling reactions. Following deprotection with piperidine, the resin-bound peptides were cleaved using TFA/TIS/H_2O. Purification was accomplished through preparative HPLC, and mass spectrometry (MS) was employed to confirm peptide identity and purity. Subsequently, the synthesized peptides were lyophilized for further utilization in the study.

2.2 Circular dichroism (CD) spectroscopy

We conducted CD spectroscopy using a Chirascan-plus spectrometer (Applied Photophysics, London, England) at 25 °C. A 1 mm quartz cuvette held the peptides, which were dissolved at 200 μg mL^{-1} in deionized (DI) water. Spectra were recorded from 190 to 260 nm after averaging three scans and subtracting the DI water baseline. CD curves were generated using the formula: $\theta = (\theta_{obs} \times 1000)/l{\cdot}c$, where θ is the mean residue ellipticity (deg cm^2 mol^{-1}), θ_{obs} is the observed ellipticity after DI water correction at a specific wavelength (mdeg), c is the peptide concentration, and l is the path length (mm).

2.3 Transmission electron microscopy (TEM)

Peptide micelle structures were analyzed using a Hitachi TEM system (HT7800, Japan). Peptide solutions (100 μg mL^{-1}) were deposited on carbon-coated 230-mesh copper grids, air-dried, and negatively stained with 2% uranyl acetate before TEM examination.

2.4 Dynamic light scattering (DLS)

Mean particle dimensions were determined using a Malvern Nano-ZS90 particle size analyzer (UK). Peptide solutions (100 μg mL^{-1}, 1 mL) were analyzed by DLS to assess the number distribution and hydrodynamic diameters (d_h). The

solvent parameters were set to the refractive index and viscosity of pure water, with an equilibration period of 5 minutes under ambient conditions. Three measurements were taken for each sample, and data analysis automatically generated size distribution based on the number distribution.

2.5 Bacteria

Bacterial strains, including *S. aureus* ATCC 25923, MRSA ATCC 43300, *E. coli* ATCC 25922, *K. pneumoniae* ATCC 13883, *P. aeruginosa* ATCC 27853, and *A. baumannii* ATCC 17978, were sourced from the American Type Culture Collection (ATCC). Vancomycin resistant *S. aureus* (VRSA) and carbapenem-resistant *A. baumannii* (CRAB) were induced as previously described.[27] In brief, minimal inhibitory concentrations (MICs) were determined according to CLSI guidelines for *S. aureus* ATCC 25923 and *A. baumannii* ATCC 17978. Survival cells at 0.5-fold MIC were used for subsequent passages over more than 20 iterations. The fold changes at the MIC were monitored to track drug resistance development. VRSA was obtained with a final MIC of 128 μg mL^{-1} against *S. aureus* ATCC 25923, and CRAB was obtained with a final MIC of 12.5 μg mL^{-1} against *A. baumannii* ATCC 17978.

2.6 Antibacterial assay *in vitro*

Antibacterial activity was assessed using a virtual colony-count assay, following established protocols.[25,28] LB agar plate colonies were cultured in LB medium for 6–8 hours at 37 °C and 200 rpm. After triple washes, the bacterial cultures were incubated for 2 hours with peptides or the control solution, followed by the addition of 2× LB medium. Bacterial growth was monitored at OD_{600} using a Spectra Max M5 microplate reader (Molecular Devices, America).

The MIC was determined following CLSI guidelines. Bacterial colonies grown on MHB agar plates were incubated in 5 mL of MHB medium at 37 °C and 200 rpm agitation. Bacterial suspensions at 2×10^6 CFU mL^{-1} were added to 96-well plates (Corning, USA) at 50 μL per well. Successive two-fold dilutions of antibiotics or peptides (50 μL per well) were followed by 100 μL of 2×MHB medium for bacterial growth. The 96-well plates were incubated at 37 °C for about 24 hours, and the OD_{600} was recorded. The MIC was defined as the lowest concentration reducing growth by over 90% compared to the positive control. The minimum bactericidal concentration (MBC) was defined as the minimum concentration of antibiotics or peptides leading to a reduction exceeding 99.9% of the initial inoculum. MIC and MBC measurements were systematically replicated and validated across three independent experiments.

2.7 Stability test

Peptide stability was assessed by determining the MIC in physiological salt solutions and serum. Peptides (50 μL) were diluted in 96-well plates, reaching a final concentration of 150 mM NaCl for salt stability and 25% serum for serum stability. *E. coli* and *S. aureus* strains were used, following MIC assay procedures.

2.8 Time-kill kinetics

A bacterial suspension at 1×10^6 CFU mL^{-1} was combined in equal parts with KR-12, Myr-KR-12N, or Myr-KR-12C (64 μg mL^{-1}). Samples were collected at set time points (0, 30, 60, 120, 240, and 360 minutes), diluted, and plated on LB agar plates. After incubation at 37 °C for 16–18 hours, viable colonies were counted for enumeration.

2.9 Outer membrane (OM) permeability assessment

To evaluate the outer membrane penetration ability of KR-12, Myr-KR-12N, and Myr-KR-12C, we used the fluorescent dye 1-*N*-phenyl naphthyl amine (NPN). All three peptides were prepared at 128 μg mL^{-1} in sterile water. *E. coli* cultures in the logarithmic growth phase were collected, washed, and resuspended to an OD_{600} of 0.2. In 96-well plates, we combined bacterial medium, 40 μM NPN, and the peptides. The vehicle group included bacterial medium, 40 μM NPN, and sterile water. The fluorescence intensity was measured every 30 seconds for 10 minutes (excitation at 350 nm, emission at 420 nm).

2.10 Inner membrane (IM) permeability assessment

To evaluate peptide penetration of the bacterial inner membrane, we used *ortho*-nitrophenyl-β-galactoside (ONPG). KR-12, Myr-KR-12N, and Myr-KR-12C (128 μg mL^{-1}) were initially dissolved in sterile water. *E. coli* cultures in the logarithmic growth phase were collected, washed, and resuspended in 1.5 mM ONPG solution. This bacterial suspension (50 μL per well) was added to sterile 96-well plates. Peptides (50 μL per well) or sterile water (50 μL per well) for the vehicle group were also added. OD_{420} was measured at 5-minute intervals using a microplate reader for over 90 minutes.

2.11 Flow cytometry

E. coli in the log-phase (37 °C) were collected by centrifugation (10 min, 4000 rpm), washed thrice, and resuspended at 1×10^6 CFU mL^{-1}. KR-12, Myr-KR-12N, and Myr-KR-12C (128 μg mL^{-1}) were mixed with bacterial medium and incubated at 37 °C for 2 hours. Following the centrifugation and washing steps, propidium iodide (PI) solution (50 μg mL^{-1}) was added and incubated (15 min, 37 °C, dark). Subsequently, centrifugation, washing, and resuspension in PBS (400 μL) were performed. Flow cytometry data were acquired using a BD Canto II with a 488 nm laser excitation wavelength.

2.12 Scanning electron microscopy (SEM)

Peptide effects on *E. coli* morphology were observed *via* SEM (SU-8010, Hitachi, Japan). Bacteria were incubated with peptides (100 μg mL^{-1}) or a vehicle for 2 hours. After centrifugation at 4000 rpm (10 min) and two PBS washes, samples were fixed in 2.5% glutaraldehyde (overnight, 4 °C). Further PBS washing and incubation in 1% OsO4 in PBS (1.5 hours) followed. Dehydration using ethanol and SEM analysis were then performed.

2.13 Hemolysis assay

Freshly collected red blood cells (RBCs) were PBS-washed. Then, 20 μL of RBC suspension (8% of total volume) was mixed with 200 μL of peptides, PBS, or 1% Triton X-100 in EP tubes. Incubation was carried out at 37 °C with shaking (300 rpm) for 1 hour. After centrifugation (300*g*, 10 min), 100 μL of supernatant was combined with an equal volume of PBS and transferred to 96-well plates. Hemoglobin release was measured at OD_{576}. OD_{576} in PBS served as the negative control, while OD_{576} in 1% Triton X-100 represented 100% hemolysis. This formula is used to calculate the percentage of hemolysis: hemolysis (%) = [(OD_{576} in peptide solution − OD_{576} in PBS)/(OD_{576} in 1% Triton X-100 solution − OD_{576} in PBS)] × 100.

2.14 *E. coli* sepsis model

Each group consisted of 5 mice aged 6–8 weeks. They were lethally challenged with *E. coli* (1×10^7 CFU) through intraperitoneal injection. Following the challenge, mice were intraperitoneally administered with 0.5 mg kg^{-1} of either KR-12, Myr-KR-12N, Myr-KR-12C, the vehicle, or different doses of meropenem (MEM). Mortality was monitored at 12-hour intervals for 7 days.

To assess the bacterial load, mice aged 6–8 weeks underwent lethal *E. coli* challenges. They received 0.5 mg kg^{-1} KR-12, Myr-KR-12N, Myr-KR-12C, or the vehicle by intraperitoneal injections. After 6 hours, mice were anesthetized, and samples of peritoneal lavage fluid (PLF), blood, lungs, liver, spleen, and kidneys were collected. PLF was obtained by injecting PBS (4 mL) into the peritoneal cavity and agitating. Some organs were preserved in 4% formalin for subsequent H&E staining. Meanwhile, the remaining lungs, liver, spleen, and kidneys were weighed, homogenized in PBS, and plated on LB agar. Enumeration of CFU was performed following overnight incubation at 37 °C.

2.15 Endotoxin septic animal model

Male C57BL/6 mice, aged 6–8 weeks, were randomly grouped with 10 mice per group. Endotoxemia was induced with intraperitoneal LPSs and D-galactosamine (18 mg per mouse) to enhance LPS susceptibility.[29,30] LPS, diluted in endotoxin-free saline, was injected at doses of 10 ng per mouse (LD90), 50 ng per mouse, or 1 μg per mouse. Immediately after LPS, mice received peritoneal injections of 0.5 mg kg^{-1} peptide or PMB in 150 μL of pyrogen-free saline. Survival was monitored every 12 hours for 72 hours, and survival patterns were statistically analyzed using Kaplan–Meier analysis.

2.16 LPS neutralization assay

Endotoxin-neutralizing peptides were evaluated using a chromogenic Limulus amebocyte lysate (LAL) assay. A fixed endotoxin concentration (1 EU mL^{-1}) was cultured in different media. Peptide solutions (1 μg mL^{-1}, 10 μg mL^{-1}, and 100 μg mL^{-1}) were placed in microtiter plates and incubated at 37 °C. Then, 50 μL of the concentrated LAL reagent was added and incubated for 10 minutes at 37 °C. The resulting solution turned yellow. The reaction was halted with 25% hydrochloric acid, and OD_{545} was recorded.

2.17 Stimulation of mouse macrophages by LPSs

Mouse peritoneal macrophages were collected after a 72-hour intraperitoneal injection of sterile thioglycolate medium (3%, EMD Chemicals, Darmstadt, Germany). Cells were cultured in DMEM with 10% fetal calf serum, 100 U mL^{-1} penicillin, and 100 μg mL^{-1} streptomycin at 37 °C with 5% CO_2 for 24 hours. In stimulation experiments, macrophages were cultured in serum-free DMEM and co-incubated with peptides/antibiotics and LPSs for 24 hours at 37 °C. Cell-free supernatants were analyzed for TNF-α and IL-6 levels using ELISA kits (MultiSciences Biotech Co., Ltd, Hangzhou, China).

2.18 Statistical analysis

Statistical significance among groups was evaluated using an independent samples t-test or one-way ANOVA with a Bonferroni test. Significance levels were defined as follows: #$p > 0.05$, *$p < 0.05$, **$p < 0.01$, and ***$p < 0.001$. Data analysis was performed using GraphPad Prism software (v. 9.0), and unless specified, each experiment was replicated three times.

2.19 Ethical approval and informed consent

The experimental animals were handled in accordance with the guidelines outlined in the "Guide for the Care and Use of Laboratory Animals". They were maintained under sterile conditions with a 12-hour light–dark cycle, and provided with autoclaved food and sterile water. Animal experiments were conducted with ethical approval granted by the Animal Care and Use Committee of Zhengzhou University, under the reference code ZZU-LAC2021032311. Experimental animals were sourced from Beijing HFK Bioscience Co., Ltd (Beijing, China).

3 Results and discussion

3.1 Design and characterization of myristoylated KR-12

The decisive factors influencing the bactericidal efficacy of antimicrobial peptides (AMPs) encompass hydrophobicity and positive charge. Augmenting their hydrophobic characteristics facilitates self-assembly into nanostructures within aqueous environments. This self-assembly process induces localized enhancement of positive charge, thereby promoting interactions between the peptides and negatively charged bacteria. As a result of this interaction, the structural integrity of bacterial cells' outer membrane (OM) and inner membrane (IM) is compromised, as illustrated in Scheme 1.

Lipidation modification of AMPs has emerged as a strategy to augment their interaction with the lipid bilayer of bacterial membranes, potentially leading to enhanced bactericidal effects and reduced likelihood of inducing drug resistance.[31,32] The serum stability of AMPs can also be positively influenced by lipidation modifications, although the choice of fatty acid chain length becomes crucial, as both short and long chains

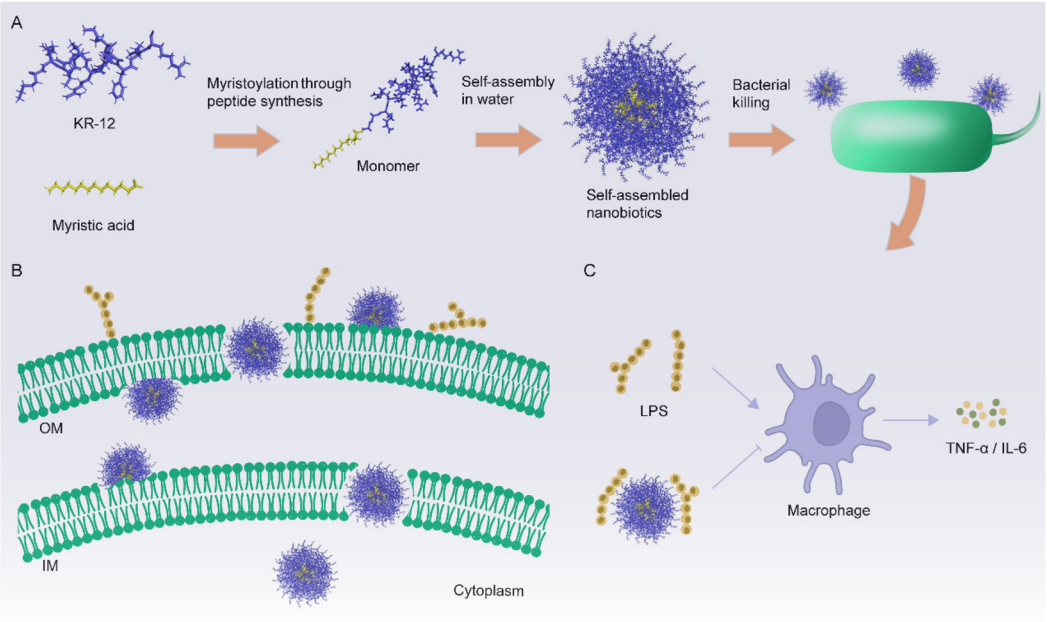

Scheme 1 (A) The generation process of nanobiotics, involving myristoylation at either the N-terminus or C-terminus of the KR-12 peptide followed by sequential nanoassembly, was schematically illustrated. (B) The antibacterial mechanism of myristoylated KR-12 nanobiotics was depicted. These nanobiotics penetrated bacterial membranes by creating pores in the bacterial outer membrane (OM) or inner membrane (IM) through binding. (C) Myristoylated KR-12 nanobiotics exhibited a high positive charge density, resulting in a strong electrostatic interaction with the negatively charged lipopolysaccharide (LPS) produced by bacteria. This led to a superior neutralizing effect, inhibiting the overproduction of inflammatory factors such as TNF-α and IL-6. In summary, the combined membrane penetration and immunomodulatory activities of myristoylated KR-12 nanobiotics contribute to their antibacterial efficacy.

impact antimicrobial activity, with excessively long chains contributing to heightened hemolytic toxicity.[33] Additionally, lipidation modification elevates the hydrophobicity of AMPs, promoting self-assembly into nanoparticles, thereby enhancing both bactericidal efficacy and stability.[32] To enhance the assembly process in aqueous settings, we made modifications to the hydrophobic nature of KR-12, a crucial step given its pronounced water solubility.[8] This entailed the introduction of myristic acid, a 14-carbon saturated fatty acid, at either its N-terminus or C-terminus. Myristic acid's unique properties, notably its capacity to form stable hydrophobic interactions and facilitate effective self-assembly in aqueous environments, thus enhancing nanostructure formation. Extensive experimental validation of myristic acid modification in previous studies, supported by empirical evidence, affirming its efficacy in enhancing self-assembly and antimicrobial properties.[25] To ensure that the fatty acids did not impact the conformation of KR-12, three glycine (Gly) residues were incorporated as linkers between the peptide and fatty acid moieties. Glycine was chosen due to the absence of an R motif. The N-terminus of KR-12 featured a free amino group, allowing for direct attachment to myristic acid. However, the C-terminus of KR-12 lacked such an amino group, necessitating the inclusion of a lysine (Lys) residue containing two free amino groups, in addition to the three Gly residues at the C-terminus. This strategic increase in local positive charge was projected to foster nanoparticle formation and enhance antibacterial capabilities.[34]

Through solid-phase peptide synthesis (SPPS), we chemically synthesized KR-12 and subsequently extended it either at its N-terminus with a Gly–Gly–Gly extension or at its C-terminus with a Gly–Gly–Gly–Lys linker. This process yielded two myristoylated variants of KR-12: Myr-KR-12N and Myr-KR-12C, respectively. Confirmation of successful synthesis was ascertained through mass spectrometry (MS) analysis (Fig. S1–S3†), with all peptides purified to a purity level exceeding 95%, determined *via* HPLC analysis (Fig. S4–S6†). Table 1 provides a comprehensive overview of structures, molecular weights, and both theoretically predicted and experimentally measured molecular weights of the peptides. The close concordance between the measured and theoretical molecular weights affirmed the successful execution of the synthesis process. In aqueous solutions, the distinct gradients of hydrophobicity among the peptides were effectively reflected in their respective retention times in HPLC. KR-12, Myr-KR-12C, and Myr-KR-12N exhibited retention times of 10.62, 12.93, and 14.22 minutes, respectively, thus implying the hydrophobic hierarchy: KR-12 < Myr-KR-12N < Myr-KR-12C.

Following confirmation of successful peptide synthesis, we proceeded to analyze their secondary structures using circular dichroism (CD) spectroscopy. In deionized water (DI water), myristoylated KR-12 exhibited distinctive spectral features, characterized by a negative peak at around 208 nm and 222 nm followed by a positive peak at approximately 195 nm, indicative of α-helical structures. Notably, a comparative ana-

Table 1 Amino acid sequence and essential physicochemical parameters of KR-12, Myr-KR-12N, and Myr-KR-12C

Peptide	Sequence[a]	Measured molecular weight	Theoretical molecular weight	Retention times[b] (min)	Purity	Net charge
KR-12	KRIVQRIKDFLR-NH2	1572.05	1571.95	10.62	>95%	+4
Myr-KR-12N	Myr-GGGKRIVQRIKDFLR-NH2	1952.12	1952.48	14.22	>95%	+4
Myr-KR-12C	KRIVQRIKDFLRGGGK-Myr	2081.76	2081.65	12.93	>95%	+5

[a] Myr indicated myristic acid. [b] HPLC solvent A consists of 0.1% trifluoroacetic acid in 100% acetonitrile, while solvent B comprises 0.1% trifluoroacetic acid in 100% water. The gradient elution profile is programmed as follows: 0.01 min: 5% A + 95% B; 25 min: 70% A + 30% B; and 30 min: 90% A + 10% B.

lysis of CD spectra between myristoylated KR-12 and native KR-12 revealed no substantial disparities (Fig. 1A). This observation underscored that myristoylation had minimal impact on the peptides' secondary structure. CD spectra of myristoylated KR-12 closely mirrored those of native KR-12. Further analysis in DI water demonstrated that the secondary structures of myristoylated KR-12 were nearly identical to native KR-12, characterized by similar proportions of α-helices, β-hairpins, and random coils (Table S1†).

To investigate the self-assembly behavior of the two myristoylated KR-12 derivatives, we employed transmission electron microscopy (TEM). Upon mixing Myr-KR-12N or Myr-KR-12C with DI water at a concentration of 100 μg mL^{-1}, spherical structures spontaneously formed (Fig. 1B). Subsequent analysis using dynamic light scattering (DLS) revealed the mean hydrodynamic diameter (d_h) values of 136.0 ± 27.7 nm and 202.6 ± 48.6 nm for Myr-KR-12N and Myr-KR-12C, respectively, with a relatively low polydispersity index (Fig. 1C and D). Furthermore, based on the TEM and DLS results, it was evident that the particle size of Myr-KR-12N was smaller than that of Myr-KR-12C. This disparity in particle size could be attributed to the heightened hydrophobicity of Myr-KR-12N in comparison with Myr-KR-12C (Table 1). It is well-established that the greater internal hydrophobicity of self-assembled micelles imparts a stronger stabilizing effect on nanoparticles, resulting in smaller and more uniform particle sizes.

3.2 Myristoylated KR-12 potently kills ESKAPE *in vitro*

E. faecium, *S. aureus*, *K. pneumoniae*, *A. baumannii*, *P. aeruginosa*, *and E. species*, collectively known as "ESKAPE" pathogens, constitute a group of six extensively antibiotic-resistant bacteria. They are responsible for the majority of

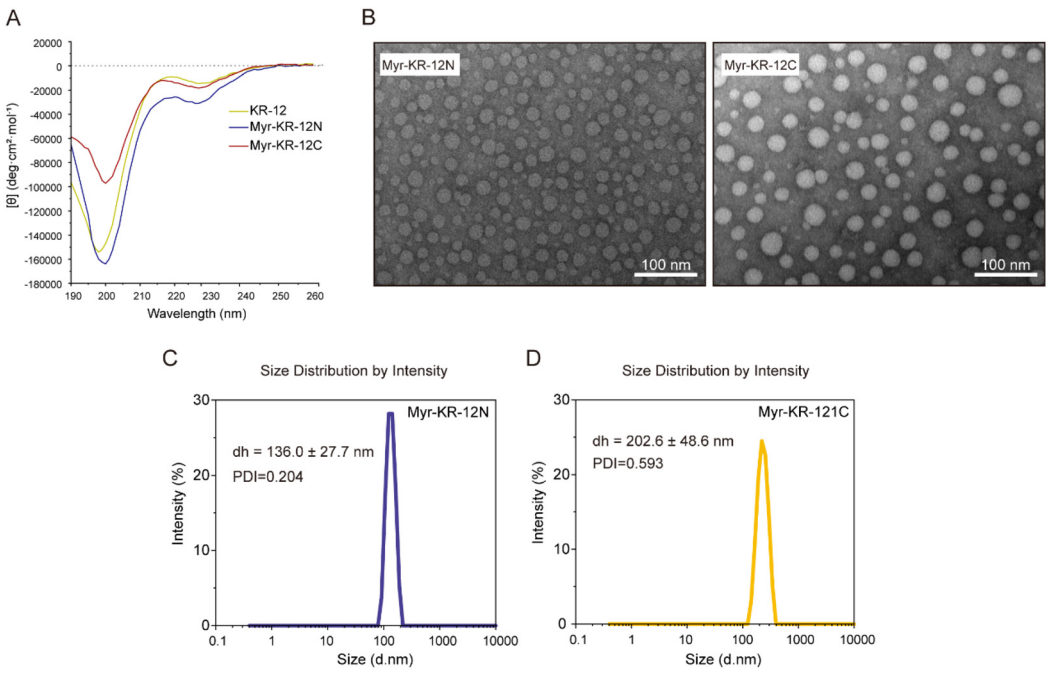

Fig. 1 (A) Circular dichroism (CD) spectroscopy was conducted on KR-12, Myr-KR-12N, and Myr-KR-12, each dissolved in deionized water at a concentration of 200 μg mL^{-1}. (B) Transmission electron microscopy (TEM) images reveal the formation of nanoparticles by Myr-KR-12N and Myr-KR-12C in deionized water at a concentration of 100 μg mL^{-1}, with a scale bar representing 100 nm. (C and D) The size distribution of Myr-KR-12N and Myr-KR-12C nanoparticles (100 μg mL^{-1}) was analyzed using dynamic light scattering (DLS), with the results presented as intensity and size distributions. Each experiment was repeated independently three times.

cases involving bacteremia and surgical-site infections within hospital settings.[25,28,35]

To evaluate the antimicrobial efficacy of KR-12, Myr-KR-12N, and Myr-KR-12C against *E. coli*, *A. baumannii*, *P. aeruginosa*, *K. pneumoniae*, *S. aureus*, and methicillin-resistant *S. aureus* (MRSA), we employed a previously established colony count method.[25,28] In brief, bacterial cultures (2×10^6 CFU mL^{-1}) were mixed with an equal volume of 2× LB medium, and their growth rates were continuously monitored using a 96-well plate reader at 37 °C. This enabled the assessment of bacterial survival following 2-hour exposure to varying peptide concentrations. As illustrated in Fig. 2, Myr-KR-12N and Myr-KR-12C exhibited more potent bactericidal activities compared to their parent peptide, KR-12. For instance, at a concentration of 12.5 μg mL^{-1}, Myr-KR-12N demonstrated a remarkable reduction in the survival of *K. pneumoniae*, exceeding 5 orders of magnitude. In contrast, Myr-KR-12C resulted in 2-order magnitude reduction under the same conditions (Fig. 2E). In comparison, KR-12 only showed a 1-order magnitude reduction at an equivalent concentration. In summary, the *in vitro* bactericidal activity highlights the broad-spectrum and enhanced potency of Myristoylated Myr-KR-12N and Myr-KR-12C nanobiotics in comparison with KR-12. Furthermore, we evaluated the antibacterial effect of the antibiotic meropenem (MEM) against the aforementioned bacteria using the same methodology. The results indicated that the *in vitro* bac-

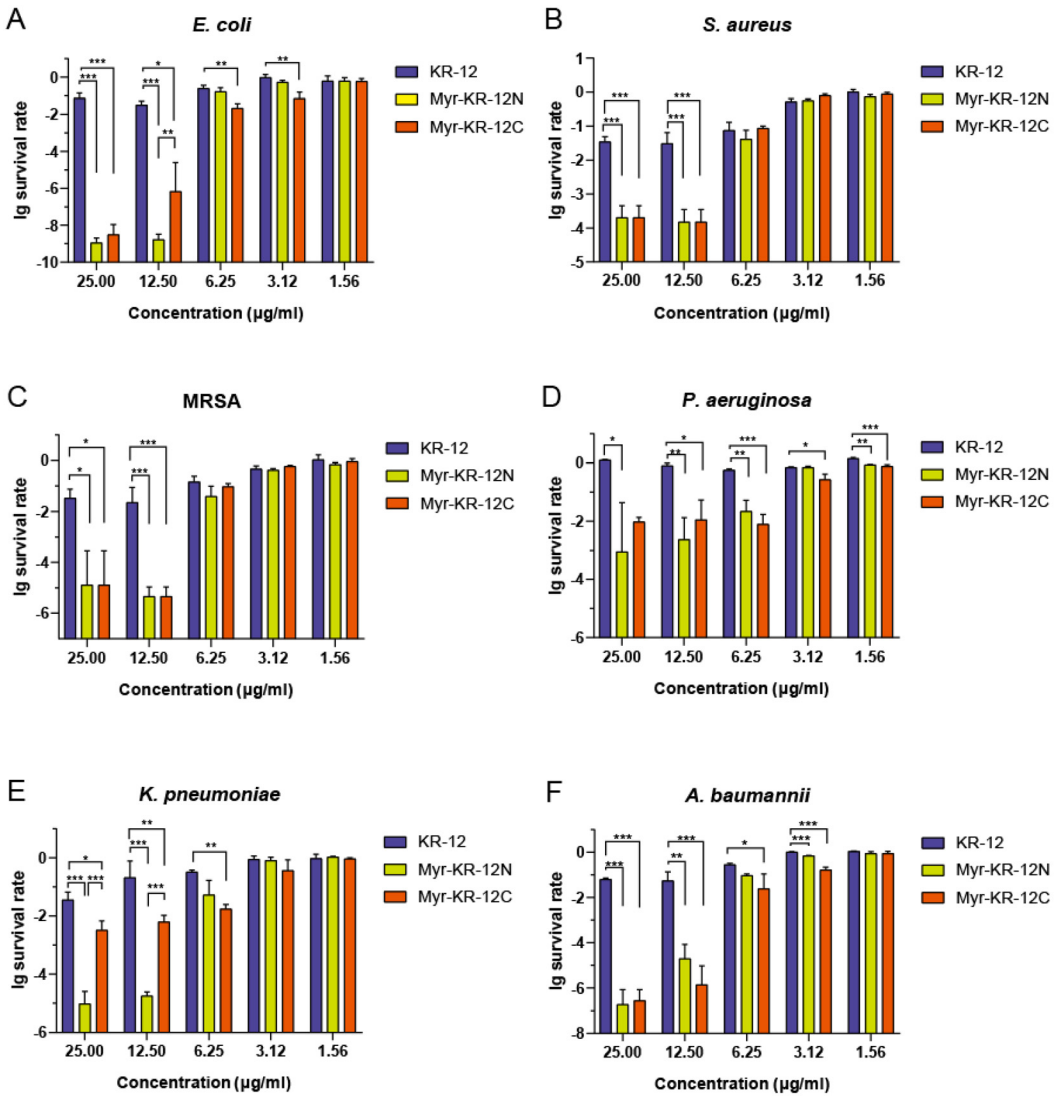

Fig. 2 Antimicrobial efficacy of KR-12, Myr-KR-12N, and Myr-KR-12C against *E. coli*, *S. aureus*, methicillin-resistant *S. aureus* (MRSA), *P. aeruginosa*, *K. pneumoniae*, and *A. baumannii* was assessed in a dose-dependent manner. Bacterial cultures (2×10^6 CFU mL^{-1}) were exposed to peptide concentrations ranging from 0.78 μg mL^{-1} to 25.00 μg mL^{-1}, and the percentage of bacterial survival (represented on a logarithmic scale) was determined by comparing colony counts from treated samples to those from mock-treated vehicle samples. Data for peptide concentrations ranging from 1.56 μg mL^{-1} to 25.00 μg mL^{-1} are presented. The results, derived from three independent experiments, are presented as the mean value with the accompanying SD. Statistical significance was determined using one-way analysis of variance (ANOVA) followed by Bonferroni's multiple comparisons test, with significance levels denoted by asterisks as follows: *$p < 0.05$, **$p < 0.01$, and ***$p < 0.001$.

tericidal effect of MEM was more pronounced than that of the nanobiotics; for instance, MEM significantly decreased the survival rate of *E. coli* by more than 5 orders of magnitude at a concentration of 0.05 μg mL^{-1} (Fig. S7†). However, animal experiments revealed that the therapeutic efficacy of myristoylated KR-12 surpassed that of MEM in septic mice (Fig. 4C). This suggests that myristoylated KR-12 may possess alternative pathways of action beyond its bactericidal activity, contributing to its superior rescue of septic mice.

Antimicrobial-resistant bacteria represent a global health concern, contributing to increased mortality due to treatment failures. In some cases, these pathogens can breach the last line of defense, rendering patients without effective antibiotic options. In our pursuit to comprehensively assess the bactericidal potential of myristoylated KR-12, we conducted minimum inhibitory concentration (MIC) and minimum bactericidal concentration (MBC) tests against the ESKAPE pathogens mentioned earlier, as well as two antibiotic-resistant strains: a vancomycin-resistant *S. aureus* (VRSA) strain and a carbapenem-resistant *A. baumannii* (CRAB) strain. The VRSA and CRAB strains were obtained through a previously established sequential passaging method.[27] As presented in Table 2, the MIC and MBC values for Myr-KR-12N and Myr-KR-12C were significantly lower than those of the parent peptide, KR-12, signifying an augmented bactericidal efficacy following our modifications. Notably, the bactericidal activities of Myr-KR-12N and Myr-KR-12C remained consistent, even when bacteria had developed resistance to conventional antibiotics, as evidenced by equivalent MIC and MBC values against *A. baumannii* and CRAB. In stark contrast, the MIC of MEM against CRAB was 10-fold higher than that against *A. baumannii*, and the MBC against CRAB was 64-fold higher than the MIC.

3.3 Stability test

AMPs often encounter challenges in salt solutions and protease-rich environments, leading to a shortened *in vivo* half-life and limited bioavailability. These obstacles significantly impede their clinical applicability. Consequently, we conducted an assessment of the resistance of KR-12, Myr-KR-12N, and Myr-KR-12C nanobiotics by determining their MIC against *E. coli*, *S. aureus*, *K. pneumoniae* and *A. baumannii* under physiological salt and serum conditions. The MIC values of KR-12, Myr-KR-12N, and Myr-KR-12C against the tested bacterial strains under 150 mM NaCl and 25% serum conditions are summarized in Table 3. Among these peptides, KR-12 exhibited no bactericidal activity in either 150 mM NaCl or 25% serum environments. In contrast, Myr-KR-12N and Myr-KR-12C maintained robust antibacterial efficacy against *E. coli*, *S. aureus*, *K. pneumoniae* and *A. baumannii* under physiological salt and serum conditions, underscoring their exceptional stability. However, a comparative analysis between Myr-KR-12N and Myr-KR-12C revealed that the antimicrobial activity of Myr-KR-12C was affected by the presence of 150 mM NaCl, while Myr-KR-12N demonstrated resilience and retained significant bactericidal activity. This discrepancy suggests that

Table 2 Minimum inhibitory concentration (MIC) and minimum bactericidal concentration (MBC) values (μg mL^{-1}) of both peptides and antibiotics

	KR-12		Myr-KR-12N		Myr-KR-12C		Meropenem		Vancomycin	
Strains	MIC	MBC	MIC	MBC	MIC	MBC	MIC	MBC	MIC	MBC
E. coli	>128	>128	8	16	16	64	0.03125	0.0625	—[a]	—
S. aureus	>128	>128	8	16	8	32	—	—	1	4
K. pneumoniae	>128	>128	4	16	8	16	0.0625	0.125	—	—
A. baumannii	>128	>128	8	16	8	32	0.125	0.25	—	—
P. aeruginosa	64	>128	16	32	32	64	0.125	0.5	—	—
MRSA[b]	>128	>128	8	32	8	32	0.25	1	—	—
VRSA[c]	>128	>128	8	16	8	32	—	—	128	>128
CRAB[d]	>128	>128	8	16	8	32	1	64	—	—

[a] Represents not measured. [b] Methicillin-resistant *S. aureus*. [c] Vancomycin resistant *S. aureus*. [d] Carbapenem-resistant *A. baumannii*.

Table 3 Stability of KR-12, Myr-KR-12N and Myr-KR-12C

		MIC in μg mL^{-1}			
AMPs	Incubation environment	*E. coli*	*S. aureus*	*K. pneumoniae*	*A. baumannii*
KR-12	MIC in water	>128	>128	>128	>128
	MIC in 150 mM NaCl	>128	>128	>128	>128
	MIC in 25% serum	>128	>128	>128	>128
Myr-KR-12N	MIC in water	8	8	4	8
	MIC in 150 mM NaCl	16	8	8	8
	MIC in 25% serum	64	64	64	32
Myr-KR-12C	MIC in water	16	8	8	8
	MIC in 150 mM NaCl	>128	>128	64	8
	MIC in 25% serum	>128	64	>128	32

the antibacterial effectiveness of Myr-KR-12C is more susceptible to physiological salt compared to its performance under aqueous conditions. In contrast, Myr-KR-12N's activity remained largely unaffected by physiological salt, in stark contrast to water. Furthermore, as presented in Table 3, the antibacterial activity of both Myr-KR-12N and Myr-KR-12C was impacted by serum exposure. This influence is likely attributed to the presence of anionic serum proteins, such as serum albumin and lipoproteins, which have the capacity to bind to AMPs, consequently diminishing their efficacy. However, it is noteworthy that Myr-KR-12N exhibited greater resilience to serum exposure compared to Myr-KR-12C, indicating its superior stability.

These findings from the experiments on physiological salt and serum stability align with *in vivo* studies, which demonstrated the enhanced therapeutic efficacy of Myr-KR-12N (Fig. 4A). The superior stability of Myr-KR-12N contributes significantly to the improvement of AMPs' half-life and bioavailability *in vivo*.

3.4 Time-kill kinetics

The kinetic profiles of bactericidal activity were assessed for KR-12, Myr-KR-12N, and Myr-KR-12C nanobiotics against *E. coli* using time-kill assays. As depicted in Fig. 3A, Myr-KR-12N, at a concentration of 64 μg mL^{-1}, achieved complete eradication of *E. coli* within a mere 2-hour incubation period. In a parallel fashion, Myr-KR-12C, at the same concentration, accomplished full bacterial clearance within 4 hours of incubation. In contrast, KR-12 exhibited a comparatively protracted bactericidal process, necessitating 6 hours of exposure at 64 μg mL^{-1}, and displaying noticeable regrowth after 4 hours of incubation. Moreover, both Myr-KR-12N and Myr-KR-12C, at a concentration of 64 μg mL^{-1}, demonstrated complete eradication of carbapenem-resistant *A. baumannii* (CRAB) within 4 hours and 6 hours, respectively (Fig. S8†). These observations indicate that Myr-KR-12N and Myr-KR-12C manifest an accelerated bactericidal effect compared to KR-12 and also possess rapid killing capabilities against drug-resistant bacteria. This enhanced bactericidal activity in Myr-KR-12N and Myr-KR-12C is postulated to be rooted in their capacity for self-assembly into nanoparticles. This self-assembly process substantially amplifies the interface of interaction between the peptides and the bacterial membrane, leading to rapid accumulation on the bacterial membrane's surface. Consequently, the peptides penetrate the membrane, trigger the release of bacterial constituents, and ultimately culminate in the demise of the bacteria.

3.5 Assessment of bacterial outer membrane (OM) permeability

Gram-negative bacteria have a robust defense mechanism due to their outer membrane (OM), predominantly composed of lipopolysaccharide (LPS), an amphiphilic macromolecule.[36] LPS creates a barrier against hydrophobic molecules and is associated with drug resistance, adhesion, and bacterial invasiveness. To assess *E. coli*'s OM permeability, we utilized the hydrophobic fluorescent dye 1-*N*-phenyl naphthyl amine (NPN), which fluoresces upon entering the hydrophobic environment when the OM is compromised. The fluorescence intensity corresponds to the extent of OM disruption. In our study, the group treated with sterile water exhibited a minimal fluorescence increase, indicating an intact OM with no permeability changes (Fig. 3B). In contrast, all tested peptides enhanced NPN fluorescence, signifying increased OM permeability. Notably, Myr-KR-12C showed a 1.5-fold increase compared to KR-12, while Myr-KR-12N displayed approximately double the fluorescence of KR-12. Furthermore, our findings reveal that both Myr-KR-12N and Myr-KR-12C possess exceptional OM disruption capacity against CRAB (Fig. S9†), suggesting that myristoylated KR-12 exhibits remarkable OM penetration even in the context of drug-resistant bacteria. Of particular significance is the outstanding permeability demonstrated by Myr-KR-12N when compared to other peptides.

3.6 Assessment of bacterial inner membrane (IM) permeability

The bacterial inner membrane, also known as the cytoplasmic membrane, is a flexible, semipermeable barrier made up of phospholipids and proteins. Maintaining the integrity of this membrane is crucial for bacterial growth and reproduction. Peptides' impact on the bacterial inner membrane can be assessed by observing changes in the medium's color. This assessment relies on the hydrolysis of *ortho*-nitrophenyl-β-galactoside (ONPG) by bacterial β-galactosidase, releasing the chromogenic compound *o*-nitrophenol (ONP) into the extracellular space when pores form in the inner membrane.[36] In Fig. 3C, the KR-12 group showed ONPG saturation in *E. coli* after about 30 minutes, similar to the control group. In contrast, the Myr-KR-12N and Myr-KR-12C groups displayed a gradual increase in absorbance intensity, indicating that Myr-KR-12N and Myr-KR-12C disrupted the inner membrane of *E. coli*, and this disruption was irreversible. These results further confirm that custom-engineered myristoylated KR-12 nanobiotics can disrupt *E. coli*'s cell membranes, with Myr-KR-12N exhibiting the most significant disruptive effect at equivalent concentrations. Moreover, myristoylated KR-12 exhibits exceptional proficiency in destabilizing the IM of CRAB (Fig. S10†). These findings highlight the remarkable membrane-disrupting capabilities of Myr-KR-12N and Myr-KR-12C nanobiotics against a spectrum of bacteria, including drug-resistant strains. This elucidation of their antimicrobial efficacy through a membrane-disrupting mechanism further emphasizes their potent bactericidal effects, particularly against drug-resistant bacteria.

3.7 Flow cytometry (FCM)

We conducted a comprehensive evaluation of the detrimental effects of KR-12 and myristoylated KR-12 nanobiotics on bacterial membranes. To assess the membrane integrity, we utilized propidium iodide (PI) staining, a fluorescence-based technique that becomes active upon binding to nucleic acids once the cytoplasmic membrane is compromised. Flow cyto-

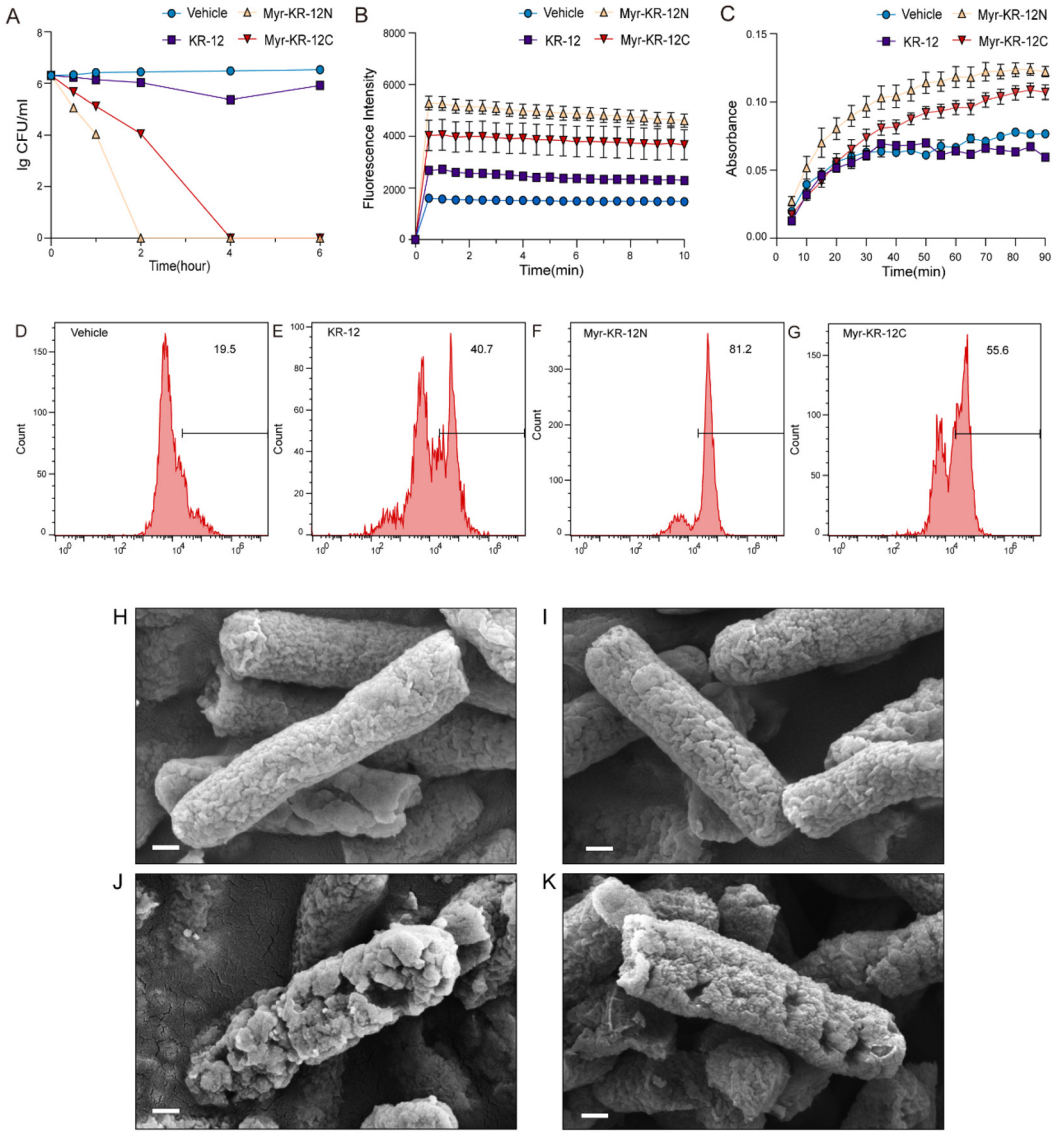

Fig. 3 (A) Time-kill kinetics of KR-12, Myr-KR-12N, and Myr-KR-12C at a concentration of 64 μg mL^{-1} against *E. coli*; (B) assessment of *E. coli*'s outer membrane permeability using the NPN uptake method with a peptide concentration of 128 μg mL^{-1}; (C) evaluation of *E. coli*'s inner membrane permeability using the ONPG reagent at a peptide concentration of 128 μg mL^{-1}; (D–G) flow cytometry analysis of *E. coli* following exposure to peptides (128 μg mL^{-1}), with the vehicle control (D) (no peptide, 19.5%), KR-12 (E) (40.7%), Myr-KR-12N (F) (81.2%), and Myr-KR-12C (G) (55.6%); (H–K) scanning electron microscopy (SEM) images of *E. coli* after a 2-hour exposure to vehicle (H), KR-12 (I), Myr-KR-12N (J), and Myr-KR-12C (K), with a peptide concentration of 100 μg mL^{-1}. Scale bars represent a length of 200 nm. Data presented here are the average values from three independent experiments, accompanied by SD.

metry (FCM) analysis was employed to quantify PI uptake in *E. coli* cells exposed to all three peptides at equimolar concentrations. In the absence of peptides, only 19.5% of the cells exhibited PI fluorescence, confirming the integrity of the bacterial membrane (Fig. 3D–G). However, following 1-hour incubation with Myr-KR-12N and Myr-KR-12C, the proportion of fluorescent bacteria, indicative of membrane disruption, increased to 81.8% and 55.6%, respectively. In contrast, only 40.7% of *E. coli* cells treated with KR-12 displayed PI staining. These observations highlight the enhanced disruptive potential of myristoylated KR-12 nanobiotics on the cytomembrane of *E. coli* compared to KR-12 in isolation, with Myr-KR-12N nanobiotic demonstrating the highest disruptive capability.

3.8 Scanning electron microscopy (SEM)

Subsequently, we employed scanning electron microscopy (SEM) to investigate the morphological changes in *E. coli* induced by peptide treatments. This analysis aimed to provide deeper insights into the antibacterial mechanisms underlying Myr-KR-12N and Myr-KR-12C nanobiotics. Exposure of *E. coli* to 100 μg mL^{-1} of KR-12 for 2 hours resulted in minimal surface alterations, whereas treatment with Myr-KR-12N or

Myr-KR-12C nanobiotics induced irregularly shaped perforations on the bacterial membrane (Fig. 3H–K). It appeared that both the inner and outer membranes were affected. Thus, the ability of KR-12, Myr-KR-12N, and Myr-KR-12C nanobiotics to induce morphological changes in *E. coli* was positively correlated with their antibacterial efficacy. Considering the established antibacterial mechanisms of Cathelicidin,[14] it is plausible that the structural disruption of bacterial membranes or walls, as evidenced by SEM results, could account for the demise of bacteria exposed to Myr-KR-12N or Myr-KR-12C nanobiotics.

Collectively, our *in vitro* assessments demonstrate that myristoylated KR-12 exhibits broad-spectrum antimicrobial properties and superior efficacy compared to its parent peptide, KR-12. Notably, myristoylated KR-12 effectively eliminates pathogens that display resistance to traditional antibiotics, offering a promising alternative for combating antibiotic-resistant bacteria.

3.9 Myr-KR-12N rescued *E. coli*-derived sepsis in mice, and Myr-KR-12N showed more potent rescuing activity than meropenem (MEM)

Motivated by the exceptional *in vitro* bactericidal efficacy, we proceeded with *in vivo* therapeutic assessments using Myr-KR-12N and Myr-KR-12C in a sepsis model. A lethal dose of *E. coli* (1×10^7 CFU per animal) was administered intraperitoneally into four distinct groups. Post-infection, three treated groups received intraperitoneal injections of 0.5 mg kg^{-1} KR-12, Myr-KR-12N, or Myr-KR-12C per septic mouse, while the control group received a vehicle (an equal volume of sterile water). Fig. 4A depicts the progression from *E. coli* infection-induced sepsis to post-infection treatment and the 72-hour survival assessment. In the vehicle-treated group, none of the mice survived beyond 24 hours after infection (Fig. 4B). Although KR-12 therapy increased the survival rate by 20%, no significant differences were observed between the vehicle-treated and KR-12-treated groups. In contrast, Myr-KR-12C nanobiotic therapy increased the survival rate to 40%, while post-treatment with Myr-KR-12N resulted in 100% survival.

Encouraged by the remarkable therapeutic efficacy of Myr-KR-12N in the *in vivo* sepsis model, we conducted a comparative study with meropenem (MEM), a potent and clinically used broad-spectrum antibiotic. Following infection with *E. coli* at a concentration of 1×10^7 CFU per mouse, septic mice were treated with Myr-KR-12N (0.5 mg kg^{-1}), MEM (0.5 mg kg^{-1}), or vehicle. Surprisingly, while MEM exhibited superior *in vitro* bactericidal activity, as evidenced by lower MIC values against ESKAPE pathogens (Table 1), only one mouse was rescued after MEM treatment, whereas Myr-KR-12N successfully rescued all mice (Fig. 4C). In a further assessment of MEM's *in vivo* bactericidal activity, mice received varying MEM doses (1, 2.5, 10, and 20 mg kg^{-1}, respectively) or a vehicle after infection. As shown in Fig. S11,† only the highest MEM dose of 20 mg kg^{-1} rescued all septic mice. These results confirm Myr-KR-12N's superior performance over the carbapenem antibiotic meropenem in treating sepsis in mice.

To gain deeper insights into its mechanisms of action in combating mouse infections, we assessed bacterial loads in organs post-treated with Myr-KR-12N or KR-12. Mice (n = 4) were subjected to a lethal *E. coli* challenge (1×10^7 CFU per mouse) and treated with 0.5 mg kg^{-1} KR-12, Myr-KR-12N, or Myr-KR-12C, or a vehicle by intraperitoneal injection. Tissue samples, blood, and peritoneal lavage fluid (PLF) were collected 6-hour after treatment for *E. coli* quantification. Fig. 5A reveals that both Myr-KR-12N and Myr-KR-12C nanobiotics effectively reduced bacterial loads in the liver, lungs, spleen, kidneys, blood, and PLF. Notably, Myr-KR-12N exhibited significantly higher efficacy in reducing bacterial burden compared to Myr-KR-12C. The severity of organ failure directly cor-

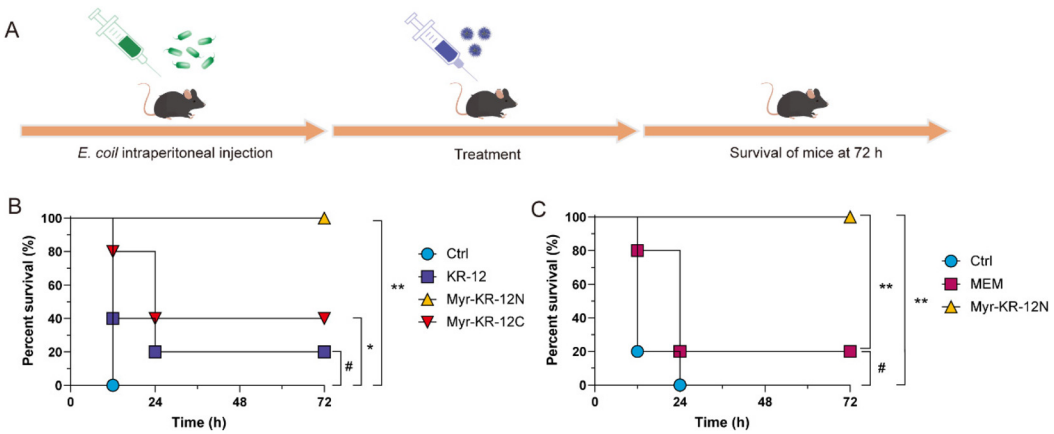

Fig. 4 Effectiveness of KR-12 and its variants in sepsis therapy. (A) Schematic representation of the treatment protocol and the 72-hour survival rate of septic mice infected with *E. coli*. (B) In each group (n = 10), every mouse received an intraperitoneal injection of 1×10^7 CFU of *E. coli*, followed by intraperitoneal treatment with vehicle, KR-12, Myr-KR-12N, or Myr-KR-12C (0.5 mg kg^{-1}) with sterile water as the solvent. (C) In a separate experiment, mice were administered with vehicle, Myr-KR-12N, or MEM (0.5 mg kg^{-1}) *via* intraperitoneal injection. Subsequently, Kaplan–Meier survival analysis was performed. Data were subjected to one-way analysis of variance (ANOVA) in conjunction with Bonferroni's multiple comparisons test. Significance levels are denoted by p values: #$p > 0.05$, *$p < 0.05$, **$p < 0.01$, and ***$p < 0.001$.

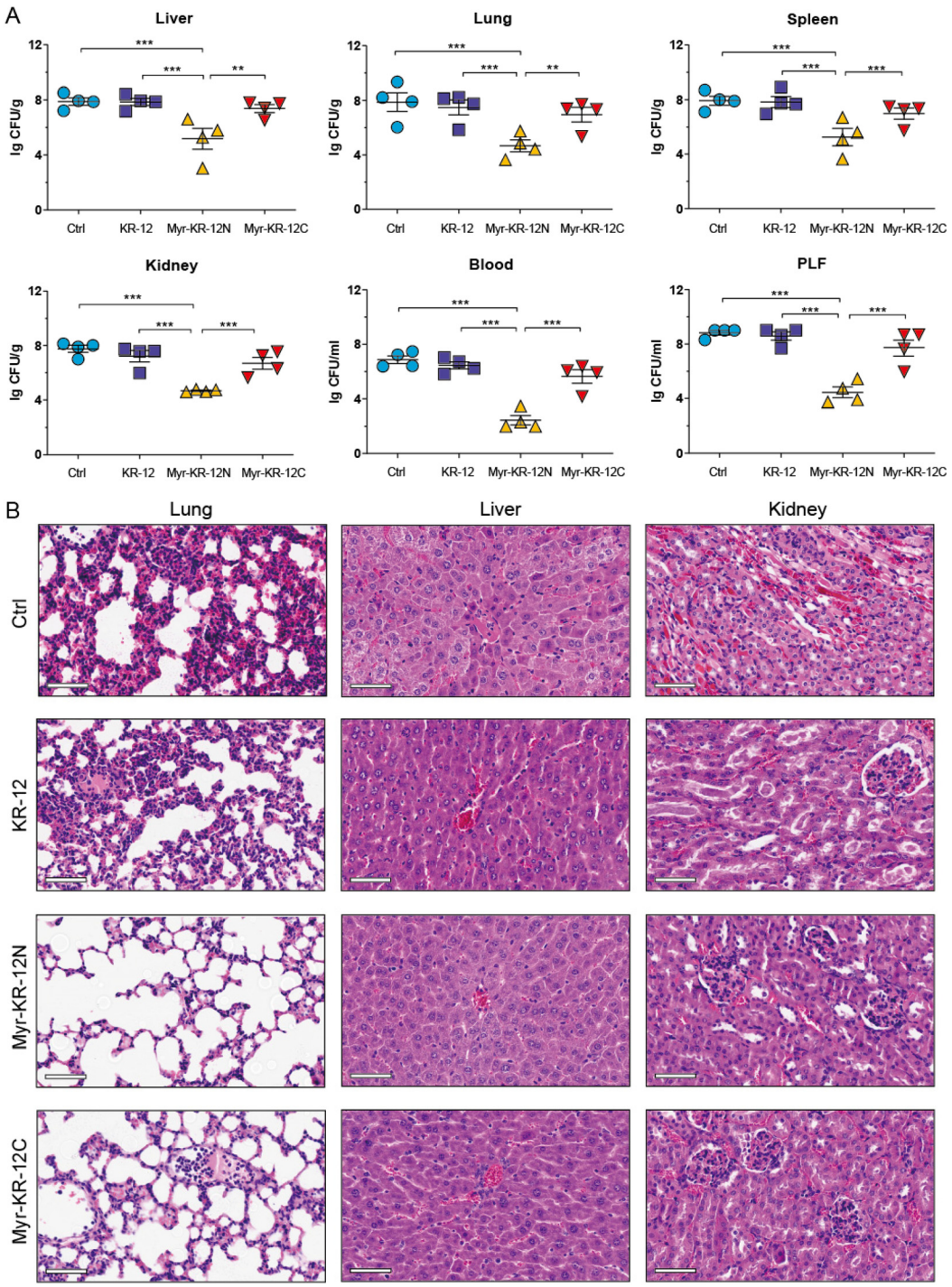

Fig. 5 Bacterial load and organ damage assessment in septic mice. After intraperitoneal challenge with 1×10^7 CFU of *E. coli*, mice in four distinct groups ($n = 4$ in each group) were treated with either a vehicle or a single dose of 0.5 mg kg^{-1} KR-12, Myr-KR-12N, or Myr-KR-12C *via* intraperitoneal injection. Seven hours post-treatment, samples of blood, peritoneal lavage fluid (PLF), liver, lungs, spleen, and kidneys were collected for bacterial quantification (A) and histological H&E staining (B). The presented results are expressed as the mean value accompanied by SEM. Statistical analysis was conducted using one-way analysis of variance (ANOVA) in conjunction with Bonferroni's multiple comparisons test. Significance levels are denoted by asterisks as follows: $^{**}p < 0.01$ and $^{***}p < 0.001$.

relates with the grim prognosis of sepsis. In order to gain a more profound insight into organ damage, the livers, lungs, and kidneys of experimental animals were fixed and subjected to histopathological examination. As depicted in Fig. 5B, the lung in the vehicle-treated group exhibited substantial thickening of the respiratory membrane and the notable recruitment

of inflamed cells. The liver showed signs of bleeding and infiltration, while the kidneys displayed hemorrhages, brush border disappearance, and cast formation. In stark contrast, treatment with Myr-KR-12N and Myr-KR-12C nanobiotics markedly alleviated sepsis-induced tissue damage, whereas KR-12 therapy had minimal to no effect in ameliorating these abnormalities.

The cumulative results from the septic mouse model demonstrate that Myr-KR-12N nanobiotics exhibit superior therapeutic efficacy against systemic bacterial infections. Notably, this efficacy surpasses that of the meropenem, rendering it a promising candidate for clinical applications.

3.10 Myristoylated KR12 nanobiotic reduced inflammation induced by LPSs *in vitro* and rescued mice of endotoxin sepsis induced by LPSs *in vivo*

LPS, a potent trigger of inflammation, is closely associated with sepsis, where an uncontrolled LPS response can be life-threatening. While the use of antibiotics is a primary approach for sepsis, some antibiotics may inadvertently exacerbate the production of bacterial inflammatory products, such as LPSs and endotoxin, leading to rapid clinical deterioration.[37–39] To address this, we hypothesized that nanosized modified KR-12, with a highly concentrated positive charge, would exhibit enhanced electrostatic attraction to the negatively charged LPS, resulting in superior neutralization. Polymyxin B (PMB), a positively charged polypeptide antibiotic produced by Bacillus Polymyxa, is known for its LPS-neutralizing potential.[40] This is achieved by specific binding, causing LPS agglutination.[29,41] Therefore, PMB has been widely used in LPS neutralization assays. The ability to neutralize LPSs, preventing the production of inflammatory cytokines like TNF-α, is closely linked to the LPS-binding capacity of antimicrobial peptides.[15]

To assess this, we employed a chromogenic Limulus amebocyte lysate (LAL) test, revealing that both Myr-KR-12N and Myr-KR-12C had significantly superior LPS-binding capabili-

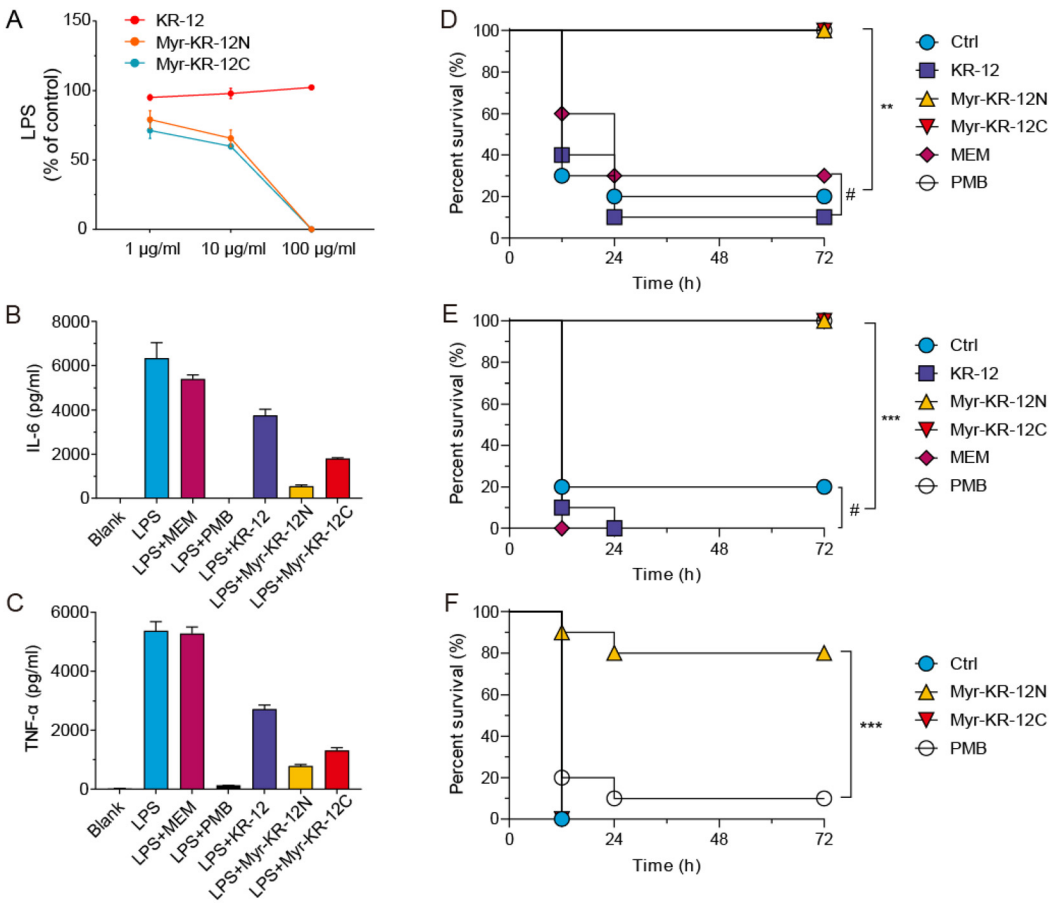

Fig. 6 LPS-binding capacity and anti-inflammatory properties of KR-12, Myr-KR-12N, Myr-KR-12C, and therapeutic efficacy in endotoxin-induced sepsis. (A) The peptides' ability to bind to LPSs was evaluated using the Limulus amebocyte lysate (LAL) assay following the manufacturer's protocol. (B and C) Murine peritoneal macrophages were cultured in the presence of 100 ng mL^{-1} LPS and 5 μg mL^{-1} peptides or antibiotics. After 24 hours of stimulation, supernatants were collected to measure IL-6 (B) and TNF-α (C) levels. (D–F) Kaplan–Meier survival analysis for galactosamine-sensitized mice (n = 10 in each group) subjected to intraperitoneal injection of 10 ng (D), 50 ng (E), or 1 μg (F) LPS, followed by treatment with vehicle, KR-12, Myr-KR-12N, Myr-KR-12C, MEM, or PMB (0.5 mg kg^{-1}). Statistical analysis was performed using one-way analysis of variance (ANOVA) in conjunction with Bonferroni's multiple comparisons test. Significance levels are denoted by p values as follows: #p > 0.05, *p < 0.05, **p < 0.01, and ***p < 0.001.

ties compared to KR-12. In experiments assessing anti-inflammatory effects in response to LPSs, macrophages exposed to peptides or antibiotics demonstrated noteworthy reductions in IL-6 and TNF-α production (Fig. 6A–C). PMB was the most effective, almost completely inhibiting both cytokines. While KR-12, Myr-KR-12N, and Myr-KR-12C also demonstrated inhibition, MEM exhibited minimal activity.

Moving from *in vitro* results to a mouse model of endotoxin sepsis, survival rates were compared. While KR-12 and MEM did not significantly increase survival, Myr-KR-12N, Myr-KR-12C, and PMB resulted in an impressive 100% survival rate at a lower LPS dose (Fig. 6D–F). Even at higher LPS doses, Myr-KR-12N displayed remarkable rescuing ability, surpassing PMB (Fig. 6E). These findings emphasize the notable reduction in endotoxin-induced immune responses by Myristoylated KR-12 nanobiotics, particularly Myr-KR-12N, which outperformed PMB in LPS neutralization activity.

In vitro endotoxin release is influenced by bacterial growth and antibiotic-induced bacterial death. Swift bacterial elimination through antibiotics results in minimal endotoxin release over 24 hours. Conversely, concurrent bacterial growth and antibiotic-induced death led to increased endotoxin release.[39] MEM showed no LPS neutralization effect and has been reported to induce high endotoxin release, possibly explaining its lower MIC against *E. coli* compared to Myr-KR-12N.[42,43] Nevertheless, Myr-KR-12N demonstrated superior efficacy in treating *E. coli* sepsis *in vivo*. Both Cathelicidin and PMB employ multifaceted mechanisms for endotoxin neutralization, including LPS interactions and bacterial membrane disruption.[29] Although Myr-KR-12N displayed weaker LPS neutralization in cellular assays than PMB, it outperformed PMB in rescuing septic mice in an *in vivo* endotoxic sepsis model. This suggests a potential multi-target mechanism of action that warrants further investigation.

3.11 Myristoylated KR-12 was found to be non-toxic

The clinical application of AMPs is hindered by potential adverse effects, particularly cytotoxicity and hemolytic activity.[44] To comprehensively assess the toxicity of nanobiotics, we conducted *in vitro* hemolytic activity evaluation,[25] covering KR-12, Myr-KR-12N, and Myr-KR-12C. Notably, neither Myr-KR-12N nor Myr-KR-12C nanobiotics exhibited significant hemolysis even at higher concentrations (Fig. S12A†). To further investigate the *in vivo* safety of Myr-KR-12N and Myr-KR-12C nanobiotics, mice received intraperitoneal injections of the Myr-KR-12N nanobiotic (5 mg kg^{-1}) or vehicle, and body weight changes were monitored for 7 days, revealing no significant differences (Fig. S12B†). In another experiment, four groups of mice received subcutaneous injections of KR-12, Myr-KR-12N, Myr-KR-12C (12 mg kg^{-1}), or vehicle every 2 hours for a total of six injections. Subsequent examinations of the liver, kidneys, and blood, along with liver and renal function tests, revealed no biochemical or histopathological abnormalities in KR-12, Myr-KR-12N, and Myr-KR-12C groups (Fig. S13 and S14†). Collectively, these experiments indicate that Myr-KR-12N and Myr-KR-12C exhibit low toxicity, making them promising candidates for clinical translation. Moreover, high-dose KR-12 treatment showed no significant pathological damage in the liver and kidneys, with no significant differences compared to the healthy control group, further supporting their safety and clinical potential.

4 Conclusion

In summary, this study has unveiled a groundbreaking nanobiotic with a unique combination of dual antimicrobial and LPS-neutralizing properties. Our nanobiotic exhibited remarkable bactericidal efficacy, surpassing meropenem (MEM), in a murine peritoneal *E. coli* infection model. This finding underscores its potential as effective treatment for bacterial infections. Moreover, in a murine LPS-induced sepsis model, our nanobiotic outperformed polymyxin B (PMB), a well-established endotoxin-neutralizing agent, in terms of LPS-neutralizing capabilities. Given the pivotal role of LPS-driven inflammation in sepsis pathogenesis, our nanobiotic's ability to neutralize LPSs, in conjunction with its potent bactericidal action, offers a promising strategy for mitigating sepsis.

It is crucial to underscore that while antibiotics are potent in eradicating bacteria, they can inadvertently exacerbate sepsis by inducing the release of LPSs through bacterial growth and lysis. In stark contrast, our nanobiotic not only eliminates bacteria effectively but also ameliorates LPS-induced inflammation by neutralizing LPSs. This dual-action approach is both elegant and effective, offering a potential breakthrough in the fight against sepsis. These findings open the door to future clinical translations, marking a significant step toward the development of innovative therapies for sepsis and bacterial infections.

In conclusion, this innovative nanobiotic presents an exciting frontier in the field of sepsis research and antimicrobial therapy. Further studies and clinical trials will be crucial in realizing its full potential and ultimately improving the outcomes for patients battling sepsis and bacterial infections.

Author contributions

Ruyi Lei, Chujun Yang, and Yaqi Sun designed the study, performed the experimental work and wrote the original manuscript, and Chujun Yang provided manuscript revision; Dejian Li, Liman Hao, and Yang Li performed the data collection and data analysis; Shuijing Wu and Hui Li contributed to the development of figures; Xiangming Fang and Ruyi Lei contributed to obtaining financial support for the research; Xiangming Fang and Chao Lan conducted an extensive literature review in the relevant field, ensuring the scientific rigor and novelty of the study. They also supervised the research project.

Conflicts of interest

There are no conflicts to declare.

Acknowledgements

This study was supported by programs from the Key R&D Program of Zhejiang Grant 2022C03163 (to X. Fang), the National Natural Science Foundation of China Grant 81902008 (to R. Lei), and the Medical Scientific and Technology Project of Henan Province Grant LHGJ20190210 (to R. Lei).

References

1 J. Moretti, B. Jia, Z. Hutchins, S. Roy, H. Yip, J. Wu, M. Shan, S. R. Jaffrey, J. Coers and J. M. Blander, *Nat. Immunol.*, 2022, **23**, 705–717.
2 L. Evans, A. Rhodes, W. Alhazzani, M. Antonelli, C. M. Coopersmith, C. French, F. R. Machado, L. McIntyre, M. Ostermann, H. C. Prescott, C. Schorr, S. Simpson, W. J. Wiersinga, F. Alshamsi, D. C. Angus, Y. Arabi, L. Azevedo, R. Beale, G. Beilman, E. Belley-Cote, L. Burry, M. Cecconi, J. Centofanti, A. C. Yataco, J. De Waele, R. P. Dellinger, K. Doi, B. Du, E. Estenssoro, R. Ferrer, C. Gomersall, C. Hodgson, M. H. Møller, T. Iwashyna, S. Jacob, R. Kleinpell, M. Klompas, Y. Koh, A. Kumar, A. Kwizera, S. Lobo, H. Masur, S. McGloughlin, S. Mehta, Y. Mehta, M. Mer, M. Nunnally, S. Oczkowski, T. Osborn, E. Papathanassoglou, A. Perner, M. Puskarich, J. Roberts, W. Schweickert, M. Seckel, J. Sevransky, C. L. Sprung, T. Welte, J. Zimmerman and M. Levy, *Intensive Care Med.*, 2021, **47**, 1181–1247.
3 A. Monserrat-Martinez, Y. Gambin and E. Sierecki, *Int. J. Mol. Sci.*, 2019, **20**, 1225.
4 A. Perner, A. C. Gordon, D. De Backer, G. Dimopoulos, J. A. Russell, J. Lipman, J. U. Jensen, J. Myburgh, M. Singer, R. Bellomo and T. Walsh, *Intensive Care Med.*, 2016, **42**, 1958–1969.
5 R. E. Hancock and H. G. Sahl, *Nat. Biotechnol.*, 2006, **24**, 1551–1557.
6 H. Jenssen, P. Hamill and R. E. Hancock, *Clin. Microbiol. Rev.*, 2006, **19**, 491–511.
7 G. Wang, X. Li and Z. Wang, *Nucleic Acids Res.*, 2009, **37**, D933–D937.
8 D. S. J. Ting, R. W. Beuerman, H. S. Dua, R. Lakshminarayanan and I. Mohammed, *Front. Immunol.*, 2020, **11**, 983.
9 R. Spohn, L. Daruka, V. Lázár, A. Martins, F. Vidovics, G. Grézal, O. Méhi, B. Kintses, M. Számel, P. K. Jangir, B. Csörgő, Á. Györkei, Z. Bódi, A. Faragó, L. Bodai, I. Földesi, D. Kata, G. Maróti, B. Pap, R. Wirth, B. Papp and C. Pál, *Nat. Commun.*, 2019, **10**, 4538.
10 M. Magana, M. Pushpanathan, A. L. Santos, L. Leanse, M. Fernandez, A. Ioannidis, M. A. Giulianotti, Y. Apidianakis, S. Bradfute, A. L. Ferguson, A. Cherkasov, M. N. Seleem, C. Pinilla, C. de la Fuente-Nunez, T. Lazaridis, T. Dai, R. A. Houghten, R. E. W. Hancock and G. P. Tegos, *Lancet Infect. Dis.*, 2020, **20**, e216–e230.
11 W. Li, F. Separovic, N. M. O'Brien-Simpson and J. D. Wade, *Chem. Soc. Rev.*, 2021, **50**, 4932–4973.
12 Y. Han, M. Zhang, R. Lai and Z. Zhang, *Peptides*, 2021, **146**, 170666.
13 I. Nagaoka, H. Tamura and J. Reich, *Int. J. Mol. Sci.*, 2020, **21**, 5973.
14 K. E. Ridyard and J. Overhage, *Antibiotics*, 2021, **10**, 650.
15 B. Jacob, I. S. Park, J. K. Bang and S. Y. Shin, *J. Pept. Sci.*, 2013, **19**, 700–707.
16 G. Wang, *J. Biol. Chem.*, 2008, **283**, 32637–32643.
17 Y. Zhao, M. Pu, J. Zhang, Y. Wang, X. Yan, L. Yu and Z. He, *Nanoscale*, 2021, **13**, 10726–10747.
18 X. Feng, K. Sambanthamoorthy, T. Palys and C. Paranavitana, *Peptides*, 2013, **49**, 131–137.
19 A. Giacometti, O. Cirioni, R. Ghiselli, F. Mocchegiani, G. D'Amato, R. Circo, F. Orlando, B. Skerlavaj, C. Silvestri, V. Saba, M. Zanetti and G. Scalise, *Am. J. Respir. Crit. Care Med.*, 2004, **169**, 187–194.
20 J. L. Narayana, R. Golla, B. Mishra, X. Wang, T. Lushnikova, Y. Zhang, A. Verma, V. Kumar, J. Xie and G. Wang, *ACS Infect. Dis.*, 2021, **7**, 1795–1808.
21 E. Kamysz, E. Sikorska, M. Jaśkiewicz, M. Bauer, D. Neubauer, S. Bartoszewska, W. Barańska-Rybak and W. Kamysz, *Int. J. Mol. Sci.*, 2020, **21**, 887.
22 S. Gunasekera, T. Muhammad, A. A. Strömstedt, K. J. Rosengren and U. Göransson, *ChemBioChem*, 2018, **19**, 931–939.
23 B. Mishra, R. F. Epand, R. M. Epand and G. Wang, *RSC Adv.*, 2013, **3**, 19560–19571.
24 P. P. Kalelkar, M. Riddick and A. J. García, *Nat. Rev. Mater.*, 2022, **7**, 39–54.
25 R. Lei, J. Hou, Q. Chen, W. Yuan, B. Cheng, Y. Sun, Y. Jin, L. Ge, S. A. Ben-Sasson, J. Chen, H. Wang, W. Lu and X. Fang, *ACS Nano*, 2018, **12**, 5284–5296.
26 T. Mori, M. Hazekawa, M. Yoshida, T. Nishinakagawa, T. Uchida and D. Ishibashi, *Int. J. Pharm.*, 2021, **606**, 120891.
27 A. de Breij, M. Riool, R. A. Cordfunke, N. Malanovic, L. de Boer, R. I. Koning, E. Ravensbergen, M. Franken, T. van der Heijde, B. K. Boekema, P. H. S. Kwakman, N. Kamp, A. El Ghalbzouri, K. Lohner, S. A. J. Zaat, J. W. Drijfhout and P. H. Nibbering, *Sci. Transl. Med.*, 2018, **10**, eaan4044.
28 B. Ericksen, Z. Wu, W. Lu and R. I. Lehrer, *Antimicrob. Agents Chemother.*, 2005, **49**, 269–275.
29 A. B. Schromm, L. Paulowski, Y. Kaconis, F. Kopp, M. Koistinen, A. Donoghue, S. Keese, C. Nehls, J. Wernecke, P. Garidel, E. Sevcsik, K. Lohner, S. Sanchez-Gomez, G. Martinez-de-Tejada, K. Brandenburg, M. Brameshuber, G. J. Schütz, J. Andrä and T. Gutsmann, *Proc. Natl. Acad. Sci. U. S. A.*, 2021, **118**, e2101721118.
30 C. Galanos, M. A. Freudenberg and W. Reutter, *Proc. Natl. Acad. Sci. U. S. A.*, 1979, **76**, 5939–5943.
31 F. Armas, A. Di Stasi, M. Mardirossian, A. A. Romani, M. Benincasa and M. Scocchi, *Int. J. Mol. Sci.*, 2021, **22**, 7959.

32 B. C. Lin, A. D. Hung, W. Singleton, K. K. Darmawan, R. Moses, B. C. Yao, H. K. Wu, A. Barlow, S. Marc-Antoine, A. J. Sloan, M. A. Hossain, J. D. Wade, Y. N. Hong, N. M. O'Brien-Simpson and W. Y. Li, *Aggregate*, 2023, DOI: 10.1002/agt2.329.
33 E. Grimsey, D. W. P. Collis, R. Mikut and K. Hilpert, *Biochim. Biophys. Acta, Biomembr.*, 2020, **1862**, 183195.
34 L. Liu, K. Xu, H. Wang, P. K. Tan, W. Fan, S. S. Venkatraman, L. Li and Y. Y. Yang, *Nat. Nanotechnol.*, 2009, **4**, 457–463.
35 G. Luo, J. Zhang, H. Wang, Y. Sun, B. Cheng, Z. Xu, Y. Zhang, H. Li, W. Lu, E. Nemeth, T. Ganz and X. Fang, *Proc. Natl. Acad. Sci. U. S. A.*, 2022, **119**, e2117283119.
36 M. Niu, X. Gu, J. Yang, H. Cui, X. Hou, Y. Ma, C. Wang and G. Wei, *ACS Nano*, 2023, **17**, 6292–6316.
37 P. Skorup, L. Maudsdotter, E. Tano, M. Lipcsey, M. Castegren, A. Larsson and J. Sjölin, *Crit. Care Med.*, 2018, **46**, e634–e641.
38 P. M. Lepper, T. K. Held, E. M. Schneider, E. Bölke, H. Gerlach and M. Trautmann, *Intensive Care Med.*, 2002, **28**, 824–833.
39 A. Thorsted, E. Tano, K. Kaivonen, J. Sjölin, L. E. Friberg and E. I. Nielsen, *Antimicrob. Agents Chemother.*, 2020, **64**, e02070-19.
40 A. P. Zavascki, L. Z. Goldani, J. Li and R. L. Nation, *J. Antimicrob. Chemother.*, 2007, **60**, 1206–1215.
41 M. M. Domingues, R. G. Inácio, J. M. Raimundo, M. Martins, M. A. Castanho and N. C. Santos, *Biopolymers*, 2012, **98**, 338–344.
42 K. Fujita, I. Takata, I. Yoshida, H. Takashima and H. Sugiyama, *J. Antibiot.*, 2022, **75**, 136–145.
43 M. Tsuji, H. Matsuda, H. Miwa and S. Miyazaki, *J. Antimicrob. Chemother.*, 2003, **51**, 353–359.
44 E. Sancho-Vaello, D. Gil-Carton, P. François, E. J. Bonetti, M. Kreir, K. R. Pothula, U. Kleinekathöfer and K. Zeth, *Sci. Rep.*, 2020, **10**, 17356.